Quantum phase transitions from competing short- and long-range interactions on a π-flux lattice

Xingchuan Zhu [1], Yiqun Huang,[2] Huaiming Guo,[3,*] and Shiping Feng [2]

[1]*Interdisciplinary Center for Fundamental and Frontier Sciences, Nanjing University of Science and Technology, Jiangyin, Jiangsu 214443, People's Republic of China*

[2]*Department of Physics, Beijing Normal University, Beijing 100875, China*

[3]*School of Physics, Beihang University, Beijing 100191, China*

(Received 29 April 2022; revised 6 July 2022; accepted 22 July 2022; published 3 August 2022)

Quantum phase transitions from the cluster-charge interaction, which is composed of competing short- and long-range interactions, are investigated on a π-flux lattice by using the mean-field theory and determinant quantum Monte Carlo (DQMC) simulations. Both methods identify a plaquette-dimer phase, which develops from a finite interaction strength. While its signature in DQMC is relatively weak, an obvious antiferromagnetic transition is revealed in the spin structure factor instead. The corresponding critical interaction and exponents are readily obtained by finite-size scalings, with the plaquette-dimer structure factor that can also be well scaled. These results suggest a possible deconfined quantum critical point between the plaquette-dimer and antiferromagnetic phases driven by the cluster-charge interaction on a π-flux lattice.

DOI: 10.1103/PhysRevB.106.075109

I. INTRODUCTION

Dirac semimetal (SM) in two dimensions has attracted intense interest in condensed matter physics [1–8]. The low-energy electronic states of this class of quantum matters can be effectively described by a Dirac equation. The resulting linear dispersion relation leads to many exotic physical phenomena. Besides the well-known graphene, various two-dimensional (2D) Dirac materials have been predicted and discovered experimentally up to now [9–17].

The emergence of massless Dirac fermions is usually protected by specific lattice symmetries. When the lattice is distorted by various periodic perturbations, the Dirac semimetal can spawn interesting insulating phases. A recent key theoretical advance is to gap the Dirac semimetal with spin-orbit coupling, which has led to the discovery of time-reversal-invariant topological insulators [18–20]. Other insulating phases can be generated by introducing various kinds of dimerizations of the hopping amplitudes and charge-density-wave modulations of the on-site energies [21–23]. The above periodic orders are usually driven by interactions through spontaneous symmetry breaking. When the repulsive interactions of different ranges coexist, a rich phase diagram, composed of various charge, spin, and topological ordered phases, will be obtained[24–27]. The abundant phase transitions therein allow the system to become an ideal platform to investigate the exotic quantum criticality.

While most quantum critical behaviors can be well described by Landau's theory of phase transitions [28,29], recent theoretical studies have led to the notion that Landau's description is insufficient. In particular, a new class of phase transition, termed as deconfined quantum critical point (DQCP), is established based on 2D antiferromagnets [30–36]. DQPC occurs in a phase transition between the Néel and valence bond solid (VBS) phases. Although either a first-order phase transition or phase coexistence is expected according to Landau's theory, the actual transition is a direct second-order one, and thus should be described by the new theory, DQCP.

Deconfined quantum criticality may also exist in fermionic systems [37–42]. While the antiferromagnetic (AF) order can be induced by the on-site Hubbard repulsion, the VBS phase can be stabilized by competing short- and long-range interactions. Indeed convincing evidences of DQCP between the AF and VBS phases have been demonstrated in the extended Hubbard model of fermions on a honeycomb lattice [41,42]. The studies on DQCP in fermionic systems are much more difficult since the quantum Monte Carlo simulations are usually restricted to smaller lattice sizes than those of spin Hamiltonians. Therefore, additional specially designed interactions need to be included to stabilize the ordered phases (especially the VBS phase) in a larger parameter regime [42].

In the initial stage of modeling the strong correlation physics in twisted bilayer graphene, the cluster-charge interaction, which has a simple form and is feasible for sign-problem-free DQMC simulations, has been proposed as an effective interaction on a honeycomb lattice [43,44]. Interestingly it is found the Kekulé VBS is stabilized in a wide range of interaction strengths. Although there exists a transition from the VBS to AF phases, it is shown to be a first-order one. As the other realization of 2D Dirac semimetals, the π-flux lattice has a lattice symmetry and coordination number distinct from the honeycomb lattice [45–54]. Thus it is natural to ask what kind of VBS may be stabilized, and whether a DQCP may be realized by the cluster-charge interaction on the π-flux lattice.

*hmguo@buaa.edu.cn

In this paper, the quantum phase transitions from competing short- and long-range interactions constituting the cluster-charge interaction are investigated on a π-flux lattice. The mean-field theory predicts the appearance of plaquette-dimer phase from a finite interaction strength. While the subsequent DQMC simulations find signatures of the above SM-VBS transition, the lattice sizes accessed are not large enough to characterize the VBS transitions due to the fragility of the plaquette-dimer phase. A clear AF transition is revealed instead, whose critical interaction and exponents are estimated by finite-size scalings. Furthermore, we find the structure factor of the VBS phase can be scaled satisfactorily with the above critical values. Our results suggest a possible DQCP between the plaquette-dimer and AF phases driven by the cluster-charge interaction on a π-flux lattice.

This paper is organized as follows. Section II introduces the model we will investigate, along with our computational methodology. Section III presents the results from the mean-field theory. Section IV uses DQMC simulations to study the quantum phase transitions of the interacting Hamiltonian. Section V includes the conclusions and discussions.

II. THE MODEL AND METHOD

We start with the following Hamiltonian describing interacting spin-1/2 fermions on a π-flux lattice [51,52]:

$$H = -\sum_{\langle ij\rangle,\sigma}(t_{ij}c^{\dagger}_{i\sigma}c_{j\sigma} + \text{H.c.}) + U\sum_{\square}(Q_{\square}-2)^2, \quad (1)$$

where the sum on σ runs over spins $\sigma = \uparrow, \downarrow$, and $\langle ij\rangle$ denotes the nearest-neighbor (NN) pairs; $c^{\dagger}_{i\sigma}$ and $c_{i\sigma}$ are creation and annihilation operators of electrons with spin σ on a given site i; the cluster charge $Q_{\square} = \sum_{i\in\square}\frac{n_i}{2}$ is defined as the total charge on the four sites of each plaquette with $n_i = \sum_{\sigma} c^{\dagger}_{i\sigma}c_{i\sigma}$ the total number operator of electrons on each site; and U is the interaction strength. To avoid the cluster-charge interaction, four electrons per plaquette are energetically favored, when the system is exactly at half filling.

The first term in Eq. (1) is noninteracting, describing the electrons on a square lattice subjected to a magnetic field. The magnetic flux per plaquette is one half of a magnetic flux quantum $\Phi_0 = hc/e$. As a consequence, when an electron hopping along the four bonds constituting a plaquette is in one direction, a total phase π is picked up when it returns to the starting point. We choose the Landau gauge so that all hopping amplitudes in the x direction are $t_x = t$, while the hopping signs along the y direction are staggered, i.e., $t_y = (-1)^{i_x}t = \pm t$ (i_x represents the x coordinate of the ith site). The resulting lattice is composed of two sublattices, and the unit cell contains two sites A and B (Fig. 1). In the reciprocal space, within the reduced Brillouin zone ($|k_x| \leqslant \pi/2, |k_y| \leqslant \pi$), the noninteracting Hamiltonian can be written as

$$H_0 = \sum_{\mathbf{k}\sigma}\psi^{\dagger}_{\mathbf{k}\sigma}\mathcal{H}_0(\mathbf{k})\psi_{\mathbf{k}\sigma}, \quad (2)$$

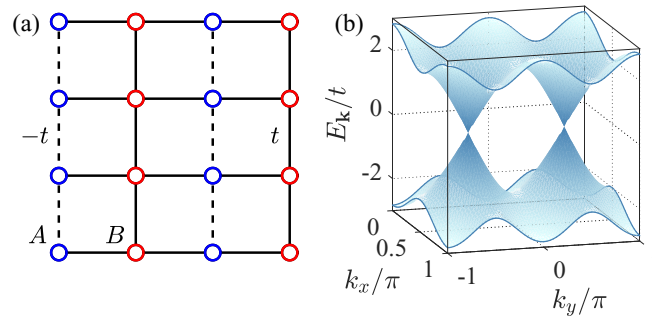

FIG. 1. (a) The π-flux model on the square lattice. The unit cell is composed of two inequivalent sites A and B. The NN hopping amplitudes may be t (solid line) or $-t$ (dashed line), depending on the directions and positions of the bonds. (b) Band structure of the π-flux square lattice with two Dirac cones at the momentum points $(k_x, k_y) = (\pi/2, \pm\pi/2)$.

with the basis $\psi_{\mathbf{k}\sigma} = (c_{A\sigma}, c_{B\sigma})^T$ and the Hamiltonian in the momentum space

$$\mathcal{H}_0(\mathbf{k}) = \begin{pmatrix} -2t\cos k_y & +2t\cos k_x \\ +2t\cos k_x & +2t\cos k_y \end{pmatrix}. \quad (3)$$

The energy spectrum is given by

$$E_{\mathbf{k}} = \pm\sqrt{4t^2(\cos^2 k_x + \cos^2 k_y)}, \quad (4)$$

which is symmetric around the Fermi level, and gapless at the two inequivalent Dirac points located at $\mathbf{K}_{\pm} = (\pi/2, \pm\pi/2)$.

The interacting term in the Hamiltonian, Eq. (1), contains various kinds of short- and long-range interactions, which is more easily seen through an expanding of the cluster-charge interaction [43],

$$U\sum_{\square}(Q_{\square}-2)^2 = 2U\sum_i n_{i\uparrow}n_{i\downarrow} + U\sum_{\langle ij\rangle} n_i n_j + \frac{1}{2}U\sum_{\langle\langle ij\rangle\rangle} n_i n_j - 7U\sum_i n_i + 4UN_s, \quad (5)$$

with N_s the total number of sites on the lattice. $\langle\langle ij\rangle\rangle$ means the next-nearest-neighbor (NNN) interactions. Thus the system includes on-site, NN, and NNN repulsions, and the interaction strength ratio from the on-site to NNN ones is $4:2:1$.

At the finite strength of U, Eq. (1) is solved numerically via DQMC, where one decouples the two-body interaction in perfect square form through the introduction of an auxiliary Hubbard-Stratonovich field, which is integrated out stochastically [55–57]. The only errors are those associated with the statistical sampling, the finite spatial lattice size, and the inverse temperature discretization. These errors are well controlled in the sense that they can be systematically reduced as needed, and further eliminated by appropriate extrapolations. At half filling, the simulations are free of sign problems due to the presence of particle-hole symmetry [58–61]. Thus we can access low enough temperatures, necessary to determine the ground-state properties on finite-size lattices. In the following, we use the inverse temperature discretization $\Delta\tau = 0.1$, and

the simulations are carried out on $L \times L$ lattices with the linear size L up to 24.

III. THE MEAN-FIELD APPROXIMATION

We first treat the Hamiltonian in Eq. (1) using the mean-field approximation, which should be helpful to identify the possible ordered quantum phases. Here we can deal with various values of the interaction strengths, thus starting from the following general interaction terms,

$$H_{\rm int} = U_0 \sum_i n_{i\uparrow} n_{i\downarrow} + V_1 \sum_{\langle ij \rangle} n_i n_j + V_2 \sum_{\langle\langle ij \rangle\rangle} n_i n_j, \quad (6)$$

where U_0, V_1, and V_2 are the strengths of the on-site, NN, and NNN interactions, respectively. All interactions are decoupled in the on-site channel as [25,26]

$$\begin{aligned} n_{i,\uparrow} n_{i,\downarrow} &= \langle n_{i,\uparrow} \rangle n_{i,\downarrow} + \langle n_{i,\downarrow} \rangle n_{i,\uparrow} - \langle n_{i,\uparrow} \rangle \langle n_{i,\downarrow} \rangle, \\ n_i n_j &= \langle n_i \rangle n_j + \langle n_j \rangle n_i - \langle n_i \rangle \langle n_j \rangle. \end{aligned} \quad (7)$$

The on-site Hubbard, NN, and NNN repulsive interactions favor antiferromagnetism, and staggered and striped charge-density waves (CDWs), respectively. We introduce three order parameters σ, ρ, and ν to characterize the above three phases. Meanwhile, the unit cell is enlarged to have four sites in the presence of the above charge and spin configurations. Then we have the following ansatz for the average density $\rho_i = \langle n_i \rangle$ on each site:

$$\begin{aligned} \rho_i &= 1 + (-1)^{i-1} \rho + (-1)^{m_i} \nu, \\ \rho_{i,\uparrow} &= \rho_i/2 + (-1)^{i-1} \sigma, \\ \rho_{i,\downarrow} &= \rho_i/2 - (-1)^{i-1} \sigma, \end{aligned} \quad (8)$$

where $i = 1, 2, 3, 4$ labels the sites in a unit cell, and $m_1 = m_2 = 0, m_3 = m_4 = 1$.

To incorporate possible valence-bond ordered phases, we also consider a bond decoupling channel for the NN interaction,

$$\begin{aligned} n_i n_j &= c_i^\dagger c_i c_j^\dagger c_j \\ &= -\langle c_i^\dagger c_j \rangle c_j^\dagger c_i - \langle c_j^\dagger c_i \rangle c_i^\dagger c_j + \langle c_j^\dagger c_i \rangle \langle c_i^\dagger c_j \rangle. \end{aligned} \quad (9)$$

While there exist various kinds of dimer patterns on the square lattice, here we focus on the spontaneous plaquette dimerization [see Fig. 2(b)], which we will demonstrate to emerge out of the competing interactions in Eq. (6) thereafter.

In the momentum space, the mean-field Hamiltonian is

$$H_{MF} = \sum_{\mathbf{k}\sigma} \psi_{\mathbf{k}}^\dagger \left[\mathcal{H}_\sigma^1(\mathbf{k}) + \mathcal{H}_\sigma^2(\mathbf{k}) \right] \psi_{\mathbf{k}} + E_0. \quad (10)$$

Here $\psi_{\mathbf{k}} = (c_{1,\mathbf{k}}, c_{2,\mathbf{k}}, c_{3,\mathbf{k}}, c_{4,\mathbf{k}})^T$ is a four-element basis. $\mathcal{H}_\sigma^1(\mathbf{k})$ is spin dependent, and for the up-spin subsystem (the formula for the down-spin copy is similar), it writes as

$$\mathcal{H}_\uparrow^1(\mathbf{k}) = \begin{bmatrix} h_{11} & t(k_x)^* & 0 & -t(k_y)^* \\ t(k_x) & h_{22} & t(k_y)^* & 0 \\ 0 & t(k_y) & h_{33} & t(k_x) \\ -t(k_y) & 0 & t(k_x)^* & h_{44} \end{bmatrix}, \quad (11)$$

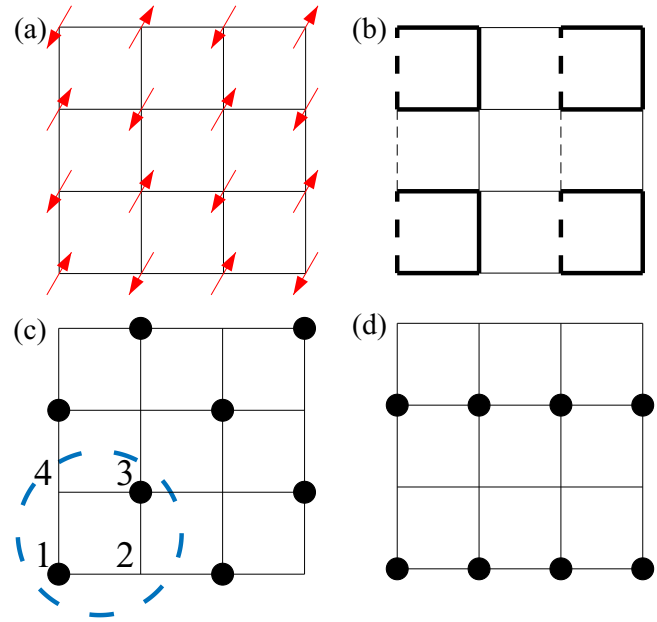

FIG. 2. Schematics of the possible ordered phases on the square lattice: (a) AF insulator, (b) plaquette dimerization, (c) staggered CDW, and (d) striped CDW. In the presence of all four orders, the unit cell is enlarged to contain four sites, each of which is marked with an integer index [see (c)]. The configurations in (a), (c), and (d) are solely favored by the on-site, NN, and NNN interactions, respectively.

with $t(k_\alpha) = t(1 + e^{ik_\alpha})$ ($\alpha = x, y$) and

$$\begin{aligned} h_{ii}^\uparrow = (-1)^{i-1} &\left(\frac{U_0}{2} - 4V_1 + 4V_2 \right) \rho \\ &+ (-1)^{m_i} \left(\frac{U_0}{2} - 4V_2 \right) \nu \\ &+ (-1)^i U_0 \sigma + \left(\frac{U_0}{2} + 4V_1 + 4V_2 \right). \end{aligned} \quad (12)$$

$\mathcal{H}_\sigma^2(\mathbf{k})$ is decoupled from the NN interaction, and does not depend on the spin index,

$$\mathcal{H}_\sigma^2(\mathbf{k}) = \begin{pmatrix} 0 & h_\chi(k_x)^* & 0 & -h_\chi(k_y)^* \\ h_\chi(k_x) & 0 & h_\chi(k_y)^* & 0 \\ 0 & h_\chi(k_y) & 0 & h_\chi(k_x) \\ -h_\chi(k_y) & 0 & h_\chi(k_x)^* & 0 \end{pmatrix}, \quad (13)$$

where $\chi_1, \chi_2 = -\langle c_{i\sigma}^\dagger c_{j\sigma} \rangle$ are for thick and thin bonds in Fig. 2(b); $h_\chi(k_\alpha) = V_1(\chi_1 + \chi_2 e^{ik_\alpha})$ with $\alpha = x, y$. Here the constant is

$$\begin{aligned} E_0 = &(8V_2 - U_0)\nu^2 + (8V_1 - U_0 - 8V_2)\rho^2 \\ &+ 4U_0\sigma^2 - U_0 - 8V_1 - 8V_2 + 4V_1 \left[\chi_1^2 + \chi_2^2 \right]. \end{aligned} \quad (14)$$

We can diagonalize the total Hamiltonian and obtain the dispersion with four branches:

$$\begin{aligned} E_i(\mathbf{k}) &= D + (-1)^i \frac{1}{\sqrt{2}} \sqrt{A + (-1)^{m_i+1} B + C}, \\ A &= a^2 + b^2 + 4(t_1^2 + t_2^2), \\ B &= (a+b) \sqrt{(a-b)^2 + 4\left(t_1^2 + t_2^2\right) + 8t_1 t_2 \cos(k_x)}, \end{aligned}$$

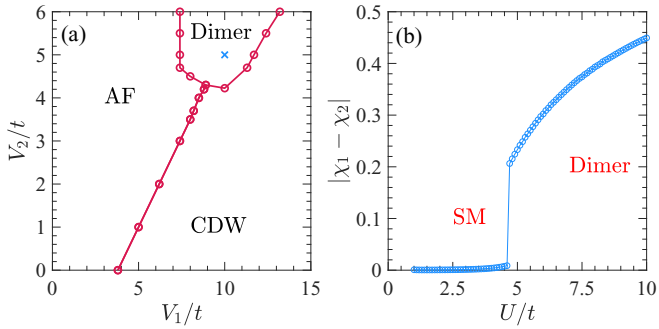

FIG. 3. (a) The phase diagram in the (V_1, V_2) plane at fixed $U_0/t = 20$. The blue cross marks the point when the interactions can be written in perfect square form of the cluster charge. (b) The order parameter $|\chi_1 - \chi_2|$, which characterizes the plaquette-dimer phase, as a function of the cluster-charge interaction U.

$$C = 4t_1t_2[\cos(k_x) + \cos(k_y)],$$
$$D = \frac{U_0}{2} + 4V_1 + 4V_2, \tag{15}$$

with

$$a = \left(\frac{U_0}{2} - 4V_1 + 4V_2\right)\rho + \left(\frac{U_0}{2} - 4V_2\right)\nu - U_0\sigma,$$
$$b = -\left(\frac{U_0}{2} - 4V_1 + 4V_2\right)\rho + \left(\frac{U_0}{2} - 4V_2\right)\nu + U_0\sigma. \tag{16}$$

Minimizing the total energy $E_{\rm tot} = \sum_{i,\mathbf{k}} E_i(\mathbf{k}) + E_0$, the order parameters of the ground state satisfy the following self-consistent equations:

$$\rho = -\frac{1}{2(8V_1 - 8V_2 - U_0)}\frac{\partial E_{\rm tot}}{\partial \rho},$$
$$\nu = -\frac{1}{2(8V_2 - U_0)}\frac{\partial E_{\rm tot}}{\partial \nu},$$
$$\sigma = -\frac{1}{8U_0}\frac{\partial E_{\rm tot}}{\partial \sigma},$$
$$\chi_1 = -\frac{1}{8V_1}\frac{\partial E_{\rm tot}}{\partial \chi_1},$$
$$\chi_2 = -\frac{1}{8V_1}\frac{\partial E_{\rm tot}}{\partial \chi_2}. \tag{17}$$

The order parameters can be obtained by numerically solving the above equations. In Fig. 3, we plot the phase diagram in the (V_1, V_2) plane at fixed $U_0/t = 20$. Three kinds of phases, including AF, CDW, and plaquette-dimer states, are revealed. In the absence of V_1 and V_2, the system is an AF insulator at $U_0/t = 20$. A phase transition from AF to CDW is driven by the NN interaction, and the critical interaction increases with V_2. When V_2 is large enough, there appears a region of plaquette-dimer phase around $V_1 = 2V_2$. In particular, at $V_1 = 2V_2 = U_0/2$ when the interactions can be written in a perfect square form of the cluster charge, the system is in the plaquette-dimer ordered state. We then investigate the quantum phase transition driven by the cluster-charge interaction U (the ratio of the interaction strengths to be $U_0 : V_1 : V_2 = 4 : 2 : 1$, and $U_0 = 2U$). As U increases, all other order parameters remain vanished except for $|\chi_1 - \chi_2|$ characterizing the plaquette dimerization. $|\chi_1 - \chi_2|$ jumps to a finite and large value at $U/t = 4.6$, marking the occurrence of a phase transition from SM to plaquette dimer.

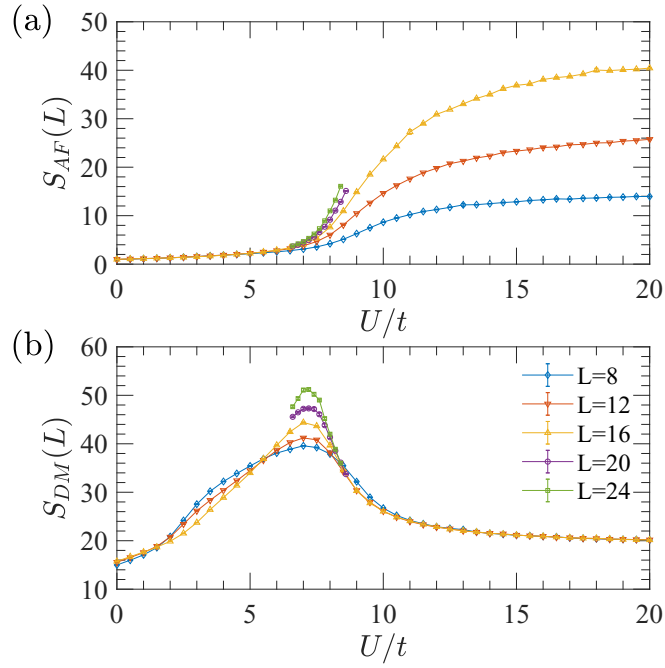

FIG. 4. The structure factors of the two kinds of orders as a function of U for various lattice sizes: (a) the AF structure factors $S_{\rm AF}(L)$; (b) the plaquette-dimer structure factor $S_{\rm DM}(L)$.

IV. RESULTS FROM THE DQMC SIMULATIONS

With the mean-field insights into the ground-state properties of the interaction Hamiltonian, Eq. (1), we next apply DQMC to unveil its physical behavior quantitatively. To characterize the AF order, we calculate the spin structure factor, which is defined by [62]

$$S(\mathbf{q}, L) = \frac{1}{N_s^2}\sum_{i,j} e^{i\mathbf{q}\cdot(\mathbf{r}_i - \mathbf{r}_j)}\langle \mathbf{S}_i \cdot \mathbf{S}_j\rangle, \tag{18}$$

where the spin operator is $\mathbf{S}_i = (S_i^x, S_i^y, S_i^z)$; N_s is the total number of sites. The antiferromagnetism has an order vector $\mathbf{q}_0 = (\pi, \pi)$, and we let $S_{\rm AF} = S(\mathbf{q}_0)$. For the plaquette-dimer phase, we define the following static structure factor:

$$S_{\rm DM}(L) = \frac{1}{N_s^2}\sum_{i,j}\sum_{\sigma,\sigma'}\langle \Delta_{i\sigma}\Delta_{j\sigma'}^\dagger\rangle, \tag{19}$$

where the bond operator writes as

$$\Delta_{i\sigma} = -[(-1)^{i_x+1}t_{i,i+x}\{(c_{i\sigma}^\dagger c_{i+x\sigma} - c_{i\sigma}^\dagger c_{i-x\sigma}) + \text{H.c.}\}$$
$$+ i(-1)^{i_y+1}t_{i,i+y}\{(c_{i\sigma}^\dagger c_{i+y\sigma} - c_{i\sigma}^\dagger c_{i-y\sigma}) + \text{H.c.}\}]. \tag{20}$$

In Fig. 4(a), we plot $S_{\rm AF}(L)$ as a function of the cluster-charge interaction U for various values of L. The AF structure factor increases continuously with U, and tends to be constant for large enough U. In addition, the saturated value increases with L. These suggest that the AF order develops at large U and the AF transition is continuous. To determine the critical

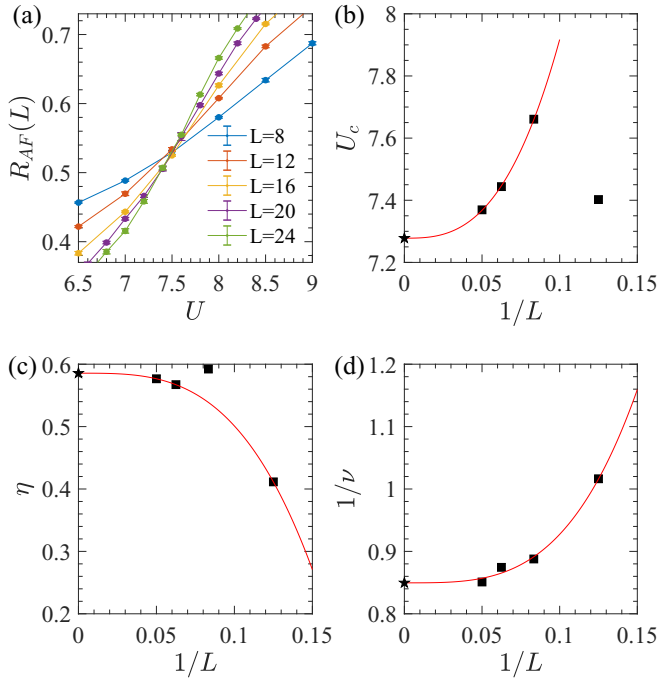

FIG. 5. (a) The RG-invariant correlation ratio of the AF structure factor as a function of the cluster-charge interaction U for various lattice sizes. (b) The critical value $U_c(L)$ determined by the crossing of two $R_{\rm AF}(L)$ curves with consecutive sizes. The anomalous dimension $\eta(L)$ (c) and the correlation function exponent ν (d) calculated according to Eq. (23). The red solid curves in (b), (c), and (d) are from polynomial fitting schemes. The fitted values in the thermodynamic limit are $U_c/t = 7.278$, $\eta = 0.586$, and $1/\nu = 0.85 \pm 0.07$, respectively.

interaction strength, we compute the renormalization-group (RG) invariant ratio of the AF structure factor [63,64]:

$$R_{\rm AF}(L) = 1 - \frac{S_{\rm AF}(\mathbf{q}_0 + \delta\mathbf{q}, L)}{S_{\rm AF}(\mathbf{q}_0, L)}, \tag{21}$$

where $\delta\mathbf{q}$ points to a NN momentum in the Brillouin zone. In the presence (absence) of long-range AF order, we have $S_{\rm AF}(\mathbf{q}_0 + \delta\mathbf{q}) \to 0[S_{\rm AF}(\mathbf{q}_0)]$, and thus $R_{\rm AF}(L) \to 1(0)$. At the critical point, the use of $R_{\rm AF}$ is advantageous as it has smaller scaling corrections than $S_{\rm AF}(\mathbf{q})$ itself. Moreover R_c has no scaling dimension, thus it will cross at the critical point U_c for different system size L. However, due to the finite-size effect, the curves of $R_{\rm AF}$ for different lattice sizes do not cross exactly at the same point [see Fig. 5(a)]. Figure 5(b) shows the critical value $U_c(L)$ determined by the crossing of two consecutive sizes, i.e., L and $L+4$. By extrapolating to the thermodynamic limit, the critical interaction is estimated to be $U_c/t = 7.278$.

The universal scaling functions describing the AF structure factor and RG-invariant correlation ratio around the quantum critical point are [42]

$$\begin{aligned} S_{\rm AF}(L) &= L^{-(d+z-2+\eta)} F_1[(U-U_c)/U_c L^{1/\nu}, L^{-b_1}], \\ R_{\rm AF}(L) &= F_2[(U-U_c)/U_c L^{1/\nu}, L^{-b_2}], \end{aligned} \tag{22}$$

where the critical exponent η is anomalous dimension, and ν is the correlation function exponent; d is the space dimension

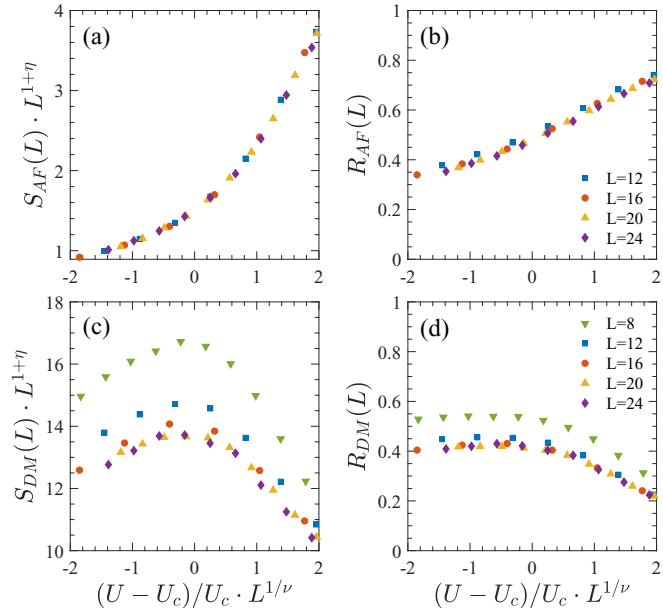

FIG. 6. Data collapses using the critical interaction and exponents determined in Fig. 5. (a) The AF structure factor, and (b) the corresponding RG-invariant correlation ratio. (c) and (d) are the plaquette-dimer structure factor and its RG-invariant ratio.

exponent, which is $d = 2$, and z is the dynamical critical exponent, which is $z = 1$ due to the Lorentz invariant; the terms L^{-b_1} and L^{-b_2} are subleading finite-size correlations; F_1 and F_2 are unknown ansatz scaling functions. Based on the above scaling function, we can extract the values of η and ν:

$$\begin{aligned} \eta(L) &= \frac{1}{\ln\left(\frac{L}{L+4}\right)} \ln\left(\frac{S_{\rm AF}(L+4)}{S_{\rm AF}(L)}\right)\Big|_{U=U_c} - (d-1), \\ \frac{1}{\nu(L)} &= \frac{1}{\ln\left(\frac{L+4}{L}\right)} \ln\left(\frac{\frac{d}{dU}R_c(L+4)}{\frac{d}{dU}R_c(L)}\right)\Big|_{U=U_c}. \end{aligned} \tag{23}$$

Figures 5(c) and 5(d) show $\eta(L)$ and $\frac{1}{\nu(L)}$ as a function of inverse lattice size, respectively. The critical exponents in the thermodynamic limit can then be obtained by fitting the data points. The anomalous dimension is determined to be $\eta = 0.586$ [65], and the correlation function exponent is $1/\nu = 0.85 \pm 0.07$. As a further check, we demonstrate the data collapses of $S_{\rm AF}(L)$ and $R_{\rm AF}(L)$ in Figs. 6(a) and 6(b), respectively, which are satisfactory for relatively large lattice sizes.

As shown in Fig. 4(b), the plaquette-dimer phase exists in a narrow region between the Dirac semimetal and the AF insulator. We also find that there is only a crossing between the curves of the largest two lattice sizes for the RG-invariant correlation ratio of the plaquette-dimer structure factor, suggesting a large finite-size effect for the plaquette-dimer order. Thus a reasonable finite-size scaling, like that performed on the AF structure factor, seems impossible for the present accessible lattice sizes. Nevertheless, we try to collapse $S_{\rm DM}(L)$ and $R_{\rm DM}(L)$ using the critical interaction and exponents obtained from the AF transition. The good collapses of the large-size data [see Figs. 6(c) and 6(d)] suggest the critical exponents from the correlation functions of the two orders

with different symmetries may be the same. Considering the continuous nature of the phase transition, it is highly expected that a DQCP exists between the plaquette-dimer and AF phases.

It is noted that there are quasirigorous bounds on critical exponents coming from the conformal bootstrap: $\eta > 0.52$ and $1/\nu < 1.957$ [66]. However, the resulting critical exponents extracted from the DQCP in bosonic systems, such as $J-Q$ spin and classical loop models [33,36,67], are in discrepancy with the above bounds. Specifically, the obtained critical exponent of the anomalous dimension is extremely small ($\eta = 0.26 \pm 0.03$ in Ref. [33]). Hence there is still a debate as to whether the Néel-VBS DQCP in the bosonic systems is really a continuous transition or a weakly first-order transition. In the present paper, we give the critical exponents of the plaquette-dimer-AF transition in the π-flux lattice, i.e., $1/\nu = 0.85 \pm 0.07$ and $\eta = 0.586$, which is not only within the conformal bootstrap bounds, but also consistent with a recent study on the same model [$\nu = 1.13(5)$, $\eta_{\mathrm{AF}} = 0.58(3)$, $\eta_{VBS} = 0.6(1)$] [68]. In addition, for the DQCP in other Dirac-fermion system [42], the obtained critical exponents for the VBS-AF transition ($\eta_{\mathrm{AF}} = 0.58 \pm 0.03$, $\eta_{VBS} = 0.59 \pm 0.02$) is in accordance with our results. All these results point to the very possible realization of the DQCP in the fermionic systems, and its profound physical properties may be further explored herein.

V. CONCLUSIONS

We investigate a specific extended Hubbard model on the π-flux lattice, in which the interaction terms can be written in a perfect square form of the cluster charge. The mean-field theory predicts a plaquette-dimer phase to occur at a finite interaction strength. While the existence of such a phase is verified by DQMC simulations, it only extends over a narrow parameter region interpolating between the Dirac semimetal and the AF insulator, thus is relatively weak for the lattice sizes accessible by DQMC. In contrast, the AF transition reflected in the spin structure factor is much more obvious, and the critical interaction and exponents are steadily obtained by finte-size scalings. We then find the plaquette-dimer structure factor of large lattice sizes can be well scaled using the above critical values. Our results reveal that a possible DQCP may be induced by the cluster-charge interaction on the π-flux lattice. Clearly, DQCP identified here needs further confirmations, either by simulating larger lattice sizes or by stabilizing the plaquette-dimer phase with additional interactions, which we leave for future studies.

Note added. Recently, we noticed a related investigation by Liao *et al.* [68].

ACKNOWLEDGMENTS

H.G. acknowledges support from the National Natural Science Foundation of China (NSFC) Grants No. 11774019 and No. 12074022, the NSAF grant in NSFC with Grant No. U1930402, the Fundamental Research Funds for the Central Universities, and the HPC resources at Beihang University. S.F. is supported by the National Key Research and Development Program of China under Grant No. 2021YFA1401803, and NSFC under Grants No. 11974051 and No. 11734002.

[1] A. H. Castro Neto, F. Guinea, N. M. R. Peres, K. S. Novoselov, and A. K. Geim, Rev. Mod. Phys. **81**, 109 (2009).
[2] A. K. Geim, Science **324**, 1530 (2009).
[3] S. M. Young and C. L. Kane, Phys. Rev. Lett. **115**, 126803 (2015).
[4] J. Cayssol, C. R. Phys. **14**, 760 (2013).
[5] J. Wang, Phys. Rev. B **95**, 115138 (2017).
[6] S. M. Young and B. J. Wieder, Phys. Rev. Lett. **118**, 186401 (2017).
[7] T. Wehling, A. Black-Schaffer, and A. Balatsky, Adv. Phys. **63**, 1 (2014).
[8] O. Vafek and A. Vishwanath, Annu. Rev. Condens. Matter Phys. **5**, 83 (2014).
[9] X.-F. Zhou and H.-T. Wang, Adv. Phys.: X **1**, 412 (2016).
[10] B. Cai, S. Zhang, Z. Hu, Y. Hu, Y. Zou, and H. Zeng, Phys. Chem. Chem. Phys. **17**, 12634 (2015).
[11] B. Wang, S. Yuan, Y. Li, L. Shi, and J. Wang, Nanoscale **9**, 5577 (2017).
[12] N. Khusnutdinov, R. Kashapov, and L. M. Woods, 2D Mater. **5**, 035032 (2018).
[13] M. Bykov, T. Fedotenko, S. Chariton, D. Laniel, K. Glazyrin, M. Hanfland, J. S. Smith, V. B. Prakapenka, M. F. Mahmood, A. F. Goncharov, A. V. Ponomareva, F. Tasnádi, A. I. Abrikosov, T. Bin Masood, I. Hotz, A. N. Rudenko, M. I. Katsnelson, N. Dubrovinskaia, L. Dubrovinsky, and I. A. Abrikosov, Phys. Rev. Lett. **126**, 175501 (2021).
[14] Y.-F. Zhang, J. Pan, H. Banjade, J. Yu, H. Lin, A. Bansil, S. Du, and Q. Yan, Nano Res. **14**, 584 (2021).
[15] J.-H. Yang, S. Song, S. Du, H.-J. Gao, and B. I. Yakobson, J. Phys. Chem. Lett. **8**, 4594 (2017).
[16] S. Cahangirov, M. Topsakal, E. Aktürk, H. Şahin, and S. Ciraci, Phys. Rev. Lett. **102**, 236804 (2009).
[17] C.-C. Liu, W. Feng, and Y. Yao, Phys. Rev. Lett. **107**, 076802 (2011).
[18] C. L. Kane and E. J. Mele, Phys. Rev. Lett. **95**, 226801 (2005).
[19] M. Z. Hasan and C. L. Kane, Rev. Mod. Phys. **82**, 3045 (2010).
[20] X.-L. Qi and S.-C. Zhang, Rev. Mod. Phys. **83**, 1057 (2011).
[21] G. W. Semenoff, V. Semenoff, and F. Zhou, Phys. Rev. Lett. **101**, 087204 (2008).
[22] C.-Y. Hou, C. Chamon, and C. Mudry, Phys. Rev. Lett. **98**, 186809 (2007).
[23] H.-M. Guo and M. Franz, Phys. Rev. B **80**, 113102 (2009).
[24] S. Raghu, X.-L. Qi, C. Honerkamp, and S.-C. Zhang, Phys. Rev. Lett. **100**, 156401 (2008).
[25] C. Weeks and M. Franz, Phys. Rev. B **81**, 085105 (2010).
[26] J. Wen, A. Rüegg, C.-C. Joseph Wang, and G. A. Fiete, Phys. Rev. B **82**, 075125 (2010).
[27] D. D. Scherer, M. M. Scherer, and C. Honerkamp, Phys. Rev. B **92**, 155137 (2015).
[28] P. Hohenberg and A. Krekhov, Phys. Rep. **572**, 1 (2015).
[29] K. G. Wilson and J. Kogut, Phys. Rep. **12**, 75 (1974).

[30] T. Senthil, L. Balents, S. Sachdev, A. Vishwanath, and M. P. A. Fisher, Phys. Rev. B **70**, 144407 (2004).
[31] T. Senthil, A. Vishwanath, L. Balents, S. Sachdev, and M. P. A. Fisher, Science **303**, 1490 (2004).
[32] C. Wang, A. Nahum, M. A. Metlitski, C. Xu, and T. Senthil, Phys. Rev. X **7**, 031051 (2017).
[33] A. W. Sandvik, Phys. Rev. Lett. **98**, 227202 (2007).
[34] R.-Z. Huang, D.-C. Lu, Y.-Z. You, Z. Y. Meng, and T. Xiang, Phys. Rev. B **100**, 125137 (2019).
[35] M. Levin and T. Senthil, Phys. Rev. B **70**, 220403(R) (2004).
[36] A. Nahum, J. T. Chalker, P. Serna, M. Ortuño, and A. M. Somoza, Phys. Rev. X **5**, 041048 (2015).
[37] Z.-X. Li, Y.-F. Jiang, S.-K. Jian, and H. Yao, Nat. Commun. **8**, 314 (2017).
[38] Z. H. Liu, M. Vojta, F. F. Assaad, and L. Janssen, Phys. Rev. Lett. **128**, 087201 (2022).
[39] X. Y. Xu, Y. Qi, L. Zhang, F. F. Assaad, C. Xu, and Z. Y. Meng, Phys. Rev. X **9**, 021022 (2019).
[40] Z. Wang, M. P. Zaletel, R. S. K. Mong, and F. F. Assaad, Phys. Rev. Lett. **126**, 045701 (2021).
[41] T. Sato, M. Hohenadler, and F. F. Assaad, Phys. Rev. Lett. **119**, 197203 (2017).
[42] Z.-X. Li, S.-K. Jian, and H. Yao, arXiv:1904.10975.
[43] X. Y. Xu, K. T. Law, and P. A. Lee, Phys. Rev. B **98**, 121406(R) (2018).
[44] Y. Da Liao, Z. Y. Meng, and X. Y. Xu, Phys. Rev. Lett. **123**, 157601 (2019).
[45] Z.-X. Li, Y.-F. Jiang, and H. Yao, New J. Phys. **17**, 085003 (2015).
[46] H.-M. Guo, L. Wang, and R. T. Scalettar, Phys. Rev. B **97**, 235152 (2018).
[47] Y. Otsuka, S. Yunoki, and S. Sorella, Phys. Rev. X **6**, 011029 (2016).
[48] Y. Otsuka and Y. Hatsugai, Phys. Rev. B **65**, 073101 (2002).
[49] C.-C. Chang and R. T. Scalettar, Phys. Rev. Lett. **109**, 026404 (2012).
[50] F. Parisen Toldin, M. Hohenadler, F. F. Assaad, and I. F. Herbut, Phys. Rev. B **91**, 165108 (2015).
[51] G. Rosenberg, B. Seradjeh, C. Weeks, and M. Franz, Phys. Rev. B **79**, 205102 (2009).
[52] Y. Jia, H. Guo, Z. Chen, S.-Q. Shen, and S. Feng, Phys. Rev. B **88**, 075101 (2013).
[53] H. Guo, E. Khatami, Y. Wang, T. P. Devereaux, R. R. P. Singh, and R. T. Scalettar, Phys. Rev. B **97**, 155146 (2018).
[54] Y. Ouyang and X. Y. Xu, Phys. Rev. B **104**, L241104 (2021).
[55] R. Blankenbecler, D. J. Scalapino, and R. L. Sugar, Phys. Rev. D **24**, 2278 (1981).
[56] S. R. White, D. J. Scalapino, R. L. Sugar, E. Y. Loh, J. E. Gubernatis, and R. T. Scalettar, Phys. Rev. B **40**, 506 (1989).
[57] S. R. White, D. J. Scalapino, R. L. Sugar, N. E. Bickers, and R. T. Scalettar, Phys. Rev. B **39**, 839 (1989).
[58] E. Y. Loh, J. E. Gubernatis, R. T. Scalettar, S. R. White, D. J. Scalapino, and R. L. Sugar, Phys. Rev. B **41**, 9301 (1990).
[59] M. Troyer and U.-J. Wiese, Phys. Rev. Lett. **94**, 170201 (2005).
[60] V. I. Iglovikov, E. Khatami, and R. T. Scalettar, Phys. Rev. B **92**, 045110 (2015).
[61] Z.-X. Li, Y.-F. Jiang, and H. Yao, Phys. Rev. B **91**, 241117(R) (2015).
[62] C. N. Varney, C.-R. Lee, Z. J. Bai, S. Chiesa, M. Jarrell, and R. T. Scalettar, Phys. Rev. B **80**, 075116 (2009).
[63] Y.-X. Zhang, W.-T. Chiu, N. C. Costa, G. G. Batrouni, and R. T. Scalettar, Phys. Rev. Lett. **122**, 077602 (2019).
[64] C. Chen, X. Y. Xu, Z. Y. Meng, and M. Hohenadler, Phys. Rev. Lett. **122**, 077601 (2019).
[65] Here we have used the fitting function $y = ax^b + c$. Due to the limited reasonable data points in Fig. 5(c), the estimation of error bar is absent.
[66] D. Poland, S. Rychkov, and A. Vichi, Rev. Mod. Phys. **91**, 015002 (2019).
[67] R. G. Melko and R. K. Kaul, Phys. Rev. Lett. **100**, 017203 (2008).
[68] Y. D. Liao, X. Y. Xu, Z. Y. Meng, and Y. Qi, arXiv:2204.04884.